Phys Chem Minerals (1995) 22:277–281

PHYSICS AND CHEMISTRY OF MINERALS

Single-Crystal X-ray Diffraction of Brucite to 14 GPa

Thomas S. Duffy, Jinfu Shu, Ho-kwang Mao, Russell J. Hemley

Geophysical Laboratory and Center for High-Pressure Research, Carnegie Institution of Washington, 5251 Broad Branch Rd, NW, Washington, DC 20015

Received December 29, 1994 / Revised, accepted March 28, 1995

Abstract. Single-crystal brucite, $Mg(OH)_2$, was studied to 14 GPa in a quasi-hydrostatic pressure medium using a diamond anvil cell and energy-dispersive synchrotron x-ray diffraction. The parameters of a third-order Birch-Murnaghan equation of state fit to the data are: $K_{0T}=42(2)$ GPa, and $(\partial K_{0T}/\partial P)_T=5.7(5)$. The bulk modulus is significantly lower than that obtained in recent shock compression and powder x-ray diffraction experiments under non-hydrostatic conditions. No evidence was found for a transition involving the Mg–O substructure over the pressure range of these experiments. This implies that the structural change previously identified at high pressure by Raman spectroscopy probably involves rearrangement of hydrogen atoms, leaving the Mg–O substructure largely unaffected.

Introduction

The alkaline earth hydroxides are important as a model system for studying structurally bound hydrogen. Brucite, $Mg(OH)_2$, serves as an analog for the complex hydrogen-bearing silicates of the Earth's crust and mantle. Brucite crystallizes in the hexagonal CdI_2 structure ($P\bar{3}m1$) (Zigan and Rothbauer 1967; Megaw 1973). The structure consists of layers of Mg–O octahedra stacked along the c axis. The hydroxyl ions are positioned along c on three-fold sites, above and below the octahedra. The interlayer forces are weak as evidenced by the large interlayer spacing and excellent cleavage. Brucite has been extensively studied at high pressure in recent years. New peaks are observed in the Raman spectrum of brucite above 4 GPa, implying there is a structural change at elevated pressure (Duffy et al. 1995a). Other studies have investigated the equation of state of brucite (Saxena 1989; Duffy et al. 1991; Fei and Mao, 1993; Parise et al. 1994; Catti et al. 1995). Reported values of the bulk modulus vary between 39 GPa to values nearly 50% larger (57 GPa). Accurate equation of state properties of brucite are needed to obtain reliable high $P-T$ thermodynamic properties of H_2O from the brucite-periclase dehydration reaction (e.g., Johnson and Walker 1993). We report here the results of a single-crystal x-ray diffraction study to obtain better constraints on the stability and equation of state of this material.

Correspondence to: T.S. Duffy

Experimental Technique

A single crystal of brucite with dimensions of approximately $180\times100\times20$ μm was loaded into a modified Merrill-Bassett diamond anvil cell. The crystal was synthesized in the same run as those used in the studies of Fei and Mao (1993) and Duffy et al. (1995a). Ambient-pressure x-ray diffraction on powder samples from this run yielded cell constants of $a=3.145(1)$ Å and $c=4.769(1)$ Å, and a unit cell volume of $V=40.851(26)$ Å^3, in good agreement with previous results for brucite (Zigan and Rothbauer 1967; Fei and Mao 1993; Redfern and Wood 1993; Catti et al. 1995).

The diamond cell had culet diameters of approximately 500 μm. The sample was placed in a 250×90-μm hole in a steel gasket held between the anvils. Several small grains of ruby were placed near the edge of the gasket. A gas loading system was used to fill the sample chamber with neon at 300 MPa. The diamond cell was then sealed and pressurized to 2 GPa. The neon provides a quasi-hydrostatic loading environment over the pressure range of these experiments. Pressures were determined using both the quasi-hydrostatic ruby fluorescence scale (Mao et al. 1986) and, at the two highest pressures, the equation of state of solid neon (Finger et al. 1981; Hemley et al. 1989).

Energy-dispersive x-ray diffraction was measured with polychromatic wiggler radiation at beamline X17C of the National Synchrotron Light Source, Brookhaven National Laboratory. The incident beam was collimated using a pair of slits to a diameter of 30 μm. Data were collected with a solid state Ge detector at fixed scattering angle. The detector was calibrated using a series of known x-ray emission lines, and the detector angle was determined ($\pm0.001°$) from diffraction of a gold standard.

The diamond cell was mounted on a goniometer and a rotation stage allowing variation of two angles (ω and χ). A computerized search was performed to orient the crystal and locate all accessible diffraction peaks at a fixed 2θ by varying these angles (Mao et al. 1988; Hu et al. 1994). Data from the following 7 classes of reflections were obtained at each pressure: (101), (100), (201), (110), (111),

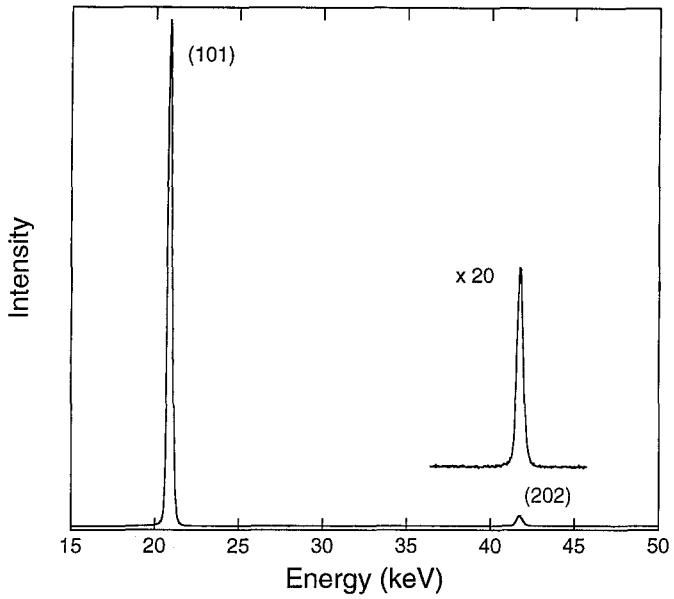

Fig. 1. Representative energy-dispersive x-ray diffraction spectrum for the (101) class of reflections for brucite at 8.0 GPa

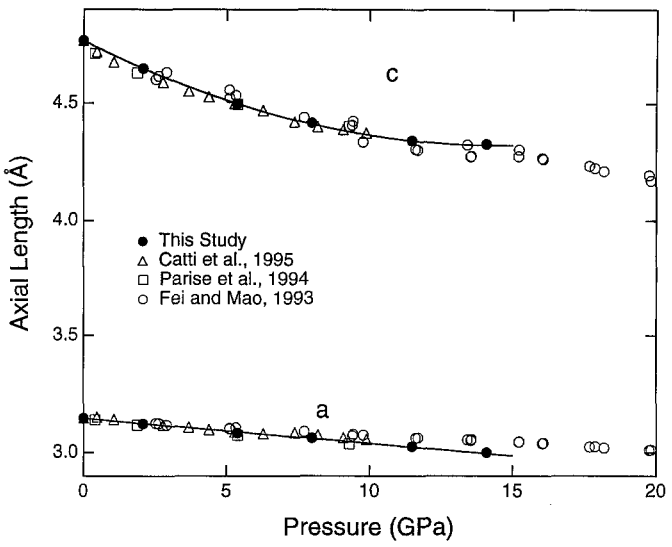

Fig. 2. *c* and *a* unit cell lengths as a function of pressure from powder x-ray, neutron, and single-crystal diffraction. The data of Parise et al. (1994) are for deuterated samples. Data of Fei and Mao (1993) at pressures higher than 20 GPa have been omitted

Table 1. Lattice parameters and volume of brucite

P(GPa)	*a*(Å)	*c*(Å)	*V*(Å^3)
2.1(1)	3.1222(3)	4.6481(32)	39.239(29)
5.4(1)	3.0832(2)	4.4977(26)	37.027(22)
8.0(1)	3.0612(3)	4.4188(30)	35.862(25)
11.5(2)	3.0261(5)	4.3424(46)	34.437(38)
14.1(1)	2.9995(4)	4.3273(36)	33.717(29)

(210), (211). All observed lines could be attributed to diffraction from brucite, gasket material, and crystalline neon. Fig. 1 shows a representative high-pressure diffraction pattern for one reflection class. Unit cell parameters were determined from measured *d* spacings using least-squares inversion. Deviations between calculated and measured *d* spacings were less than 10^{-3} Å.

Results

The lattice parameters and unit cell volumes of brucite at high pressures are shown in Table 1. For the three lowest-pressure experiments, the pressure was determined solely by ruby fluorescence. At the two highest pressures, pressures determined by the neon equation of state were lower than those obtained by ruby fluorescence by 0.3 and 0.6 GPa, respectively. The neon pressures, which were determined from 16–19 diffraction lines, are used in Table 1. The pressures from neon are believed to be more reliable than those from the ruby which was in contact with the gasket and may be affected by residual deviatoric stresses after freezing of the neon pressure medium above 4.7 GPa. However, the R_1 and R_2 ruby peaks were well-resolved at all pressures.

The unit cell parameters, *c* and *a*, as a function of pressure are shown in Fig. 2. Their pressure dependences are given by:

$$a = 3.145 - 0.0106P \quad (1)$$

$$c = 4.769 - 0.0613P + 0.0021P^2 \quad (2)$$

where *P* is the pressure in GPa. The *c* cell length decreases much more rapidly with pressure than *a* and displays a markedly non-linear pressure dependence.

The equation of state of brucite in this pressure regime has been investigated recently using powder x-ray diffraction (Fei and Mao 1993; Catti et al. 1995) and neutron diffraction of deuterated samples (Parise et al. 1994). The unit cell parameters obtained in those studies are also shown in Fig. 2. The experiment of Fei and Mao (1993) was carried out in a diamond cell without a pressure medium and reached maximum pressures of 33 GPa at room temperature and 78 GPa at 600 K. Catti et al. (1995) performed their experiments in the Paris-Edinburgh high-pressure cell (Besson et al. 1992) using equal volumes of brucite and NaCl. Parise et al. (1994) also used the Paris-Edinburgh cell, but without a pressure medium. Above 9 GPa, the *a* and *c* cell lengths of Fei and Mao (1993) lie systematically above and below those obtained here. We attribute the difference to non-hydrostatic stress states in that experiment. Brucite samples in the diamond cell show significant preferred orientation, with the *c* crystallographic axis tending to align along the axis of the cell. When material shear strength is significant, the stress along the axis of the diamond cell is larger than that in the radial direction (Singh and Balasingh 1994). This could lead to a systematically larger *a* dimension and smaller *c* dimension than those obtained under quasi-hydrostatic conditions.

The pressure dependence of the axial, or *c*/*a*, ratio is given by (Fig. 3):

$$c/a = 1.516 - 0.0143P + 0.0006P^2 \quad (3)$$

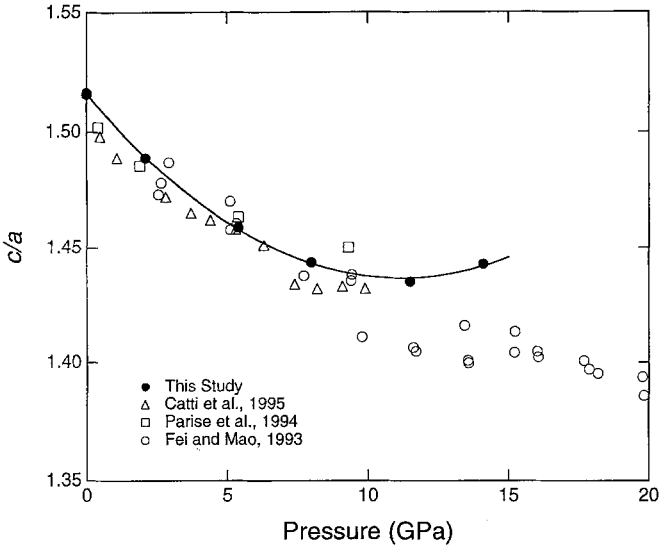

Fig. 3. Pressure dependence of the c/a ratio in brucite. Solid line is a fit to the present data

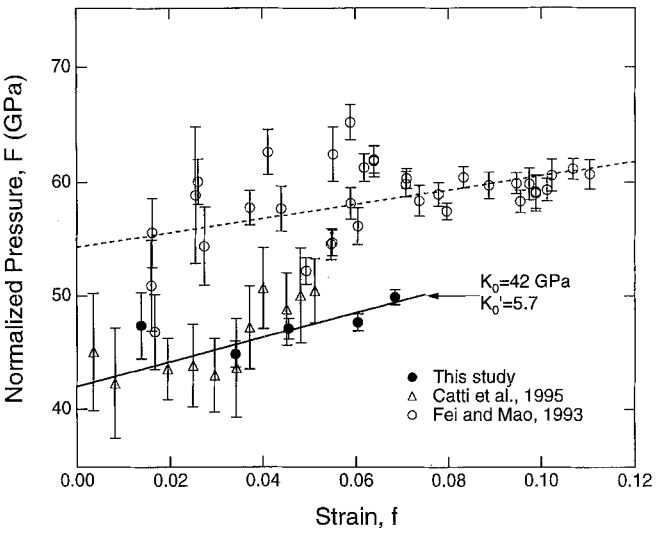

Fig. 4. Normalized pressure (F) as a function of Eulerian strain (f) for brucite static compression data. Solid line is a linear fit to the present data, and dashed line is fit to the data of Fei and Mao (1993)

The c/a ratio initially decreases strongly with pressure, but becomes nearly pressure-independent above 8 GPa, consistent with the results of earlier studies. In the powder diffraction studies, discontinuities in the c/a ratio were observed at 6–7 GPa (Catti et al.1995) and about 10 GPa (Fei and Mao 1993). No such discontinuity is observed in the single-crystal data. Such changes in the axial ratio might also arise from the non-hydrostatic stress state in those experiments. Above 10 GPa, the c/a ratio obtained in this study is about 2% larger than that of Fei and Mao (1993). The ratio reaches a minimum at 11.8 GPa and increases above this pressure. The large change in the pressure dependence of this quantity reflects the strong decrease in the compressibility of the c axis as the brucite layers are compressed (Fei and Mao 1993; Parise et al. 1994; Catti et al. 1995).

Equation of state data for brucite were evaluated using the normalized pressure (F) Eulerian strain (f) representation of the Birch-Murnaghan equation (Birch 1978). The Eulerian strain is given by:

$$f=\frac{1}{2}\left[\left(\frac{V_0}{V}\right)^{2/3}-1\right] \tag{4}$$

where V is the volume and V_0 is the ambient-pressure volume. The normalized pressure is:

$$F=\frac{P}{3f(1+2f)^{5/2}} \tag{5}$$

where P is the measured pressure. The Birch-Murnaghan equation to third order in strain energy is then given by:

$$F=K_{0T}[1+\tfrac{3}{2}(K'_{0T}-4)f] \tag{6}$$

where K_{0T} is the isothermal bulk modulus and K'_{0T} is its derivative with respect to pressure at constant temperature. A linear least squares F-f fit to compression data yields the bulk modulus and its pressure derivative.

The single-crystal brucite data are plotted in the F-f plane in Fig. 4. A weighted least squares fit yields a bulk modulus of 42(2) GPa and a pressure derivative of 5.7(5), where the numbers in parentheses are one standard deviation uncertainties in the last digit. In contrast, a fit to the earlier nonhydrostatic data to 35 GPa (Fei and Mao 1993) yields a bulk modulus nearly 30% larger [54(2) GPa] and a pressure derivative of 4.7(2). The large difference suggests that non-hydrostatic stresses may significantly affect equation of state determinations even for apparently low-strength materials like brucite. A fit to the diffraction data of Catti et al. (1995) yields $K_{0T}=39(1)$ GPa and $K'_{0T}=7.6(7)$. The bulk modulus from the present data and that of Catti et al. (1995) are generally consistent, suggesting that a mixture of 50% NaCl may reduce the effects of deviatoric stresses, particularly at low pressures. However, the pressure derivatives of the bulk modulus differ significantly. If our data are fit using pressures from ruby fluorescence rather than neon diffraction above 8 GPa, the bulk modulus is nearly unchanged [$K_{0T}=40(2)$ GPa], but the pressure derivative is considerably larger [$K'_{0T}=6.9(4)$].

Fig. 5 compares the present equation of state to shock compression data to 97 GPa (Simakov et al. 1974) and 60 GPa (Duffy et al. 1991). Reduction of the combined shock data set to a room temperature isotherm (Heinz and Jeanloz 1984) with the Grünesien parameter, $\gamma=1.16$ (Redfern and Wood 1992) yields a bulk modulus of 51(4) GPa and pressure derivative of 4.6(4). This bulk modulus also lies above that found in the present study. The shock data for brucite are highly scattered, probably resulting from sample variability. The extrapolated equation of state obtained here falls within the range of the shock data at large strains (Fig. 5). Material strength

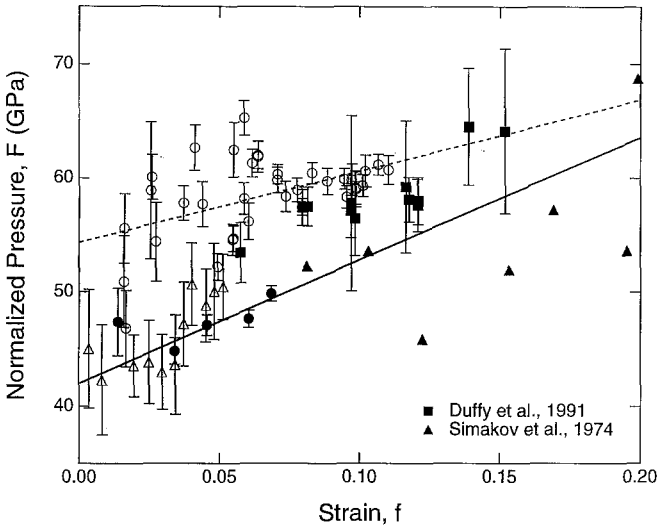

Fig. 5. Normalized pressure-stain diagram including shock compression data reduced to a room-temperature isotherm. Symbols for the static compression data are the same as in Fig. 4. Error bars for shock data of Simakov et al. (1974) are omitted because experimental uncertainties were not reported in that study

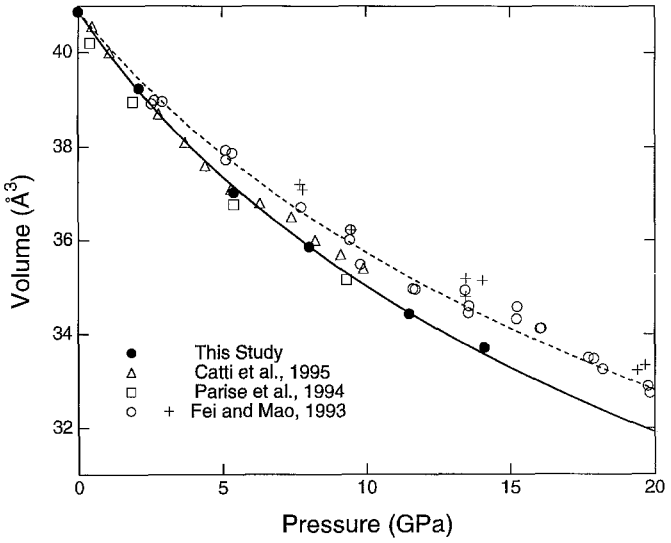

Fig. 6. Variation of unit cell volume with pressure from x-ray and neutron diffraction studies of brucite. The solid curve is the single-crystal equation of state. The dashed curve shows the equation of state of Fei and Mao (1993). Room temperature and 600 K data of Fei and Mao (1993) are shown as open circles and plus symbols, respectively, and points above 20 GPa are omitted

may also affect the schock data, and this could explain the large values of F at low strains (<0.1).

Equation-of-state data for burcite are shown in the pressure-volume plane in Fig. 6. The difference in room temperature equations of state under non-hydrostatic and quasi-hydrostatic conditions far exceeds the difference between pressure-volume data at 300 K and 600 K. At low pressures (below 5 GPa), the pressure-volumne states of Catti et al. (1995) are in good agreement with the present study, but they begin to diverge systematically at higher pressure. The NaCl pressure medium used

Table 2. Equation of State Parameters

Study	Method	K_{0T} (GPa)	K'_{0T}
This Study	Single-crystal x-ray diffraction	42(2)	5.7(5)
Saxena (1989)	Optimized phase equilibria data	57.1	4.7
Duffy et al. (1991)	Shock compression	51(4)	4.6(4)
Fei and Mao (1993)	Powder x-ray diffraction	54(2)	4.7(2)
Catti et al. (1995)	Powder x-ray diffraction	39(1)	7.6(7)

in those experiments may provide a quasi-hydrostatic environment at low pressures, but may be less effective at higher pressures due, for example, to increased strength or extrusion of the NaCl (Kinsland 1978). Thus, differences between the present experiments, Fei and Mao (1993), and Catti et al. (1995) may reflect differences in stress states in the three experiments. The present study should provide the most reliable equation of state determination for this material because of the high quality of single-crystal diffraction data and the nearly hydrostatic condition of the experiments. The bulk modulus of brucite obtained here is consistent with bounds on the modulus obtained in a recent single-crystal Brillouin scattering study of this material (D.J. Weidner, personal communication). Table 2 compares equation of state parameters for brucite derived from different compression studies.

The lack of evidence for a high-pressure phase transition is consistent with previous x-ray diffraction data up to 78 GPa and 600 K (Fei and Mao 1993; Catti et al. 1995). However, there is strong evidence from Raman spectroscopy for a structural change induced by pressure (Duffy et al. 1995a, b). Similarly, neutron diffraction studies provide evidence for H disorder in both hydrogenated and deuterated brucite at elevated pressure (Parise et al. 1994; Catti et al. 1995). The x-ray diffraction data, however, are largely insensitive to the behavior of the H atoms. Raman, neutron, and x-ray data are all consistent if there is disordering or rearrangement of atoms in the H substructure that leaves the oxygen substructure largely unaffected.

Acknowledgements. We thank J. Hu for experimental assistance and Y. Fei for providing sample material. M. Catti provided us with a preprint of his paper. This work was supported by the NSF.

References

Besson JM, Nelmes RJ, Hamel G, Loveday JS, Weill G, Hull S (1992) Neutron powder diffraction above 10 GPa. Physica B 180 & 181:907–910

Birch F (1978) Finite Strain isotherm and velocities for single-crystal and polycrystalline NaCl at high pressures and 300 K. J Geophys Res, 83:1257–1268

Catti M, Ferraris G, Hull S, Pavese A (1995) Static compression and H disorder in $Mg(OH)_2$ (brucite) to 11 GPa: a powder neutron diffraction study. Phys Chem Mineral (in press)

Duffy TS, Ahrens TJ, Lange MA (1991) The shock wave equation of state of brucite $Mg(OH)_2$. J Geophys Res, 96:14319–14330

Duffy TS, Meade C, Fei Y, Mao HK, Hemley RJ (1995a) High-pressure phase transition in brucite $Mg(OH)_2$. Am Min, 80:222–230

Duffy TS, Hemley RJ, Mao HK (1995b) Structure and bonding in hydrous minerals at high pressure: Raman spectroscopy of alkaline earth hydroxides. Deep Earth and Planetary Volatiles, edited by KA Farley, American Institute of Physics, College Park, MD, in press

Fei Y, Mao HK (1993) Static compression of $Mg(OH)_2$ to 78 GPa at high temperature and constraints on the equation of state of fluid H_2O. J Geophys Res, 98:11875–11884

Finger LW, Hazen RM, Zou G, Mao HK, Bell PM (1981) Structure and compression of crystalline neon and argon at high pressure and room temperature. Appl Phys Lett, 39:892–894

Heinz DL, Jeanloz R (1984) The equation of state of the gold calibration standard. J Appl Phys, 55:885–893

Hemley RJ, Zha CS Jephcoat AP, Mao HK, Finger LW (1989) X-ray diffraction and equation of state of solid neon to 110 GPa. Phys Rev B, 39:11820–11827

Hu J, Mao HK, Shu J, Hemley RJ (1994) High-pressure energy dispersive x-ray diffraction technique with synchrotron radiation, in High-Pressure Science and Technology, edited by SC Schmidt, JW Shaner, GA Samara, M Ross, American Institute of Physics, New York, 441–444

Johnson MC, Walker D (1993) Brucite $[Mg(OH)_2]$ dehydration and the molar volume of H_2O to 15 GPa. Am Mineral, 78:271–284

Kinsland GL (1978) The effect of the strength of materials on the interpretation of data from opposed-anvil high-pressure devices. High Temp. High Press, 10:627–639

Mao HK, Xu J, Bell PM (1986) Calibration of the ruby pressure gauge to 800 kbar under quasi-hydrostatic conditions. J Geophys Res, 91:4673–4676

Mao HK, Hemley RJ, Wu Y, Jephcoat AP, Finger LW, Zha CS, Bassett WA (1988) High-pressure phase diagram and equation of state of solid helium from single-crystal x-ray diffraction to 23.3 GPa. Phys Rev Lett, 60:2649–2652

Megaw HD (1973) Crystal Structures: A Working Approach. 563 p., WB Saunders, Philadelphia

Parise JB, Leinenweber K, Weidner DJ, Tan K, Von Dreèle RB (1994) Pressure-induced H bonding: Neutron diffraction study of brucite, $Mg(OD)_2$, to 9.3 GPa. Am Mineral. 79:193–196

Redfern SAT, Wood BJ (1992) Thermal expansion of brucite. $Mg(OH)_2$. Am Mineral, 77:1129–1132

Saxena SK (1989) Assessmant of bulk modulus, thermal expansion and heat capacity of minerals. Geochim Cosmochim Acta, 53:785–789

Simakov GV, Pavlovskiy MN, Kalashnikov NG, Trunin RF (1974) Shock compressibility of twelve minerals. Izv Solid Earth Phys, 10:11–17

Singh AK, Balasingh C (1994) The lattice strains in an opposed anvil high pressure setup. J Appl Phys, 75:4956–4962

Zigan F, Rothbauer R (1967) Neutronenbeugungsmessungen am Brucit. Neues Jahr Mineral 137–143